Research Article Vol. 2, No. 10 / October 2015 / Optica 854

Programmable photonic signal processor chip for radiofrequency applications

Leimeng Zhuang,[1,*] Chris G. H. Roeloffzen,[2] Marcel Hoekman,[3] Klaus-J. Boller,[4] and Arthur J. Lowery[1,5]

[1]Electro-Photonics Laboratory, Electrical and Computer Systems Engineering, Monash University, Clayton, VIC 3800, Australia
[2]SATRAX B.V., PO Box 456, Enschede, 7500 AL, The Netherlands
[3]LioniX BV, PO Box 456, Enschede, 7500 AL, The Netherlands
[4]Laser Physics and Nonlinear Optics group, University of Twente, PO Box 217, Enschede, 7500 AL, The Netherlands
[5]Centre for Ultrahigh-Bandwidth Devices for Optical Systems (CUDOS), Monash University, Clayton, Australia
*Corresponding author: leimeng.zhuang@monash.edu

Received 23 June 2015; revised 18 August 2015; accepted 1 September 2015 (Doc. ID 243535); published 25 September 2015

Integrated microwave photonics, an emerging technology combining radio frequency (RF) engineering and integrated photonics, has great potential to be adopted for wideband analog processing applications. However, it has been a challenge to provide photonic integrated circuits with equal levels of function flexibility as compared with their electronic counterparts. Here, we introduce a disruptive approach to tackle this need, which is analogous to an electronic field-programmable gate array. We use a grid of tunable Mach–Zehnder couplers interconnected in a two-dimensional mesh network, each working as a photonic processing unit. Such a device is able to be programmed into many different circuit topologies and thereby provide a diversity of functions. This paper provides, to the best of our knowledge, the first ever demonstration of this concept and shows that a programmable chip with a free spectral range of 14 GHz enables RF filters featuring continuous, over-two-octave frequency coverage, i.e., 1.6–6 GHz, and variable passband shaping ranging from a 55 dB extinction notch filter to a 1.6 GHz bandwidth flat-top filter.

OCIS codes: (060.5625) Radio frequency photonics; (130.3120) Integrated optics devices; (130.4815) Optical switching devices; (350.4010) Microwaves.

http://dx.doi.org/10.1364/OPTICA.2.000854

1. INTRODUCTION

Modern radio frequency (RF) systems, such as radio communications, radars, sensor networks, and terahertz (THz) imaging, demand ever-increasing bandwidth and frequency agility [1–3]. At the same time, they require devices that are small, lightweight, and low-power, exhibiting large tunability and strong immunity to electromagnetic interference. Integrated microwave photonics [4–7], an emerging technology combining RF engineering and integrated photonics, has the potential to satisfy these needs. Harnessing the large bandwidth and tunability uniquely offered by photonic devices, it enables wideband, flexible front-end analog solutions to precede digital signal processors that are currently limited to several gigahertz (GHz) analog bandwidths [8].

In integrated microwave photonics, many key RF functions have been demonstrated using on-chip photonic signal processors, including spectral filters [9–11], phase shifters [12], integrators [13], differentiators [14], pulse shapers [15,16], frequency discriminators [17,18], tunable delay lines [19,20], and beamformers [21,22]. Next to the general advantages of photonic integration in terms of device size, robustness, power efficiency, and low-cost potential [23–26], some salient works showed remarkable features such as THz processing bandwidths [27], subvolt control [28], filter extinction ratios greater than 60 dB [29], and multioctave continuous frequency shifting [19].

Although wide-ranging in application, all such demonstrations to date are based on application-specific designs of a photonic integrated circuit. A more flexible approach would be to design a universal photonic circuit whose topology can be reconfigured, post manufacture, similar to a field-programmable electronic processor, e.g., a field-programmable gate array (FPGA) [30]. This would have variable circuit parameters [9–22] but also a flexible circuit topology to suit a wide range of signal-processing functions. Recently, Pérez *et al.* presented the concept of software-defined processing in microwave photonic systems, addressing the anticipated flexibility requirements in future RF applications [31].

Here, we propose a suitable design for a FPGA-like photonic signal processor chip, as depicted in Fig. 1. The processor features full flexibility in circuit topology and full control of all circuit parameters in terms of both amplitude and phase. This unique combination is enabled by means of a grid of tunable Mach–Zehnder (MZ) couplers interconnected in a two-dimensional mesh network topology [Fig. 1(a)], with the MZ couplers being

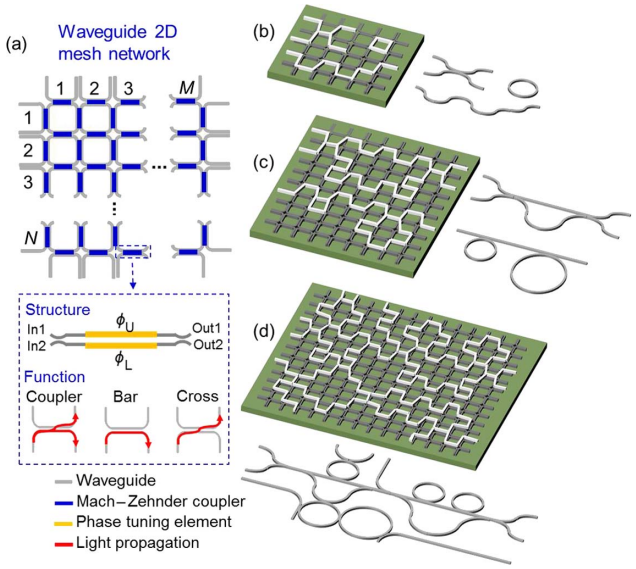

Fig. 1. (a) Schematic of a general $M \times N$ waveguide mesh network with MZ couplers being the intercell pathways. (b)–(d) Examples of implementing various circuit topologies in such mesh networks.

the intercell pathways. Each MZ coupler works as a photonic processing unit with freely programmable path-selecting, splitting/combining, and phase shifting capabilities. This makes it possible to define amplitude- and phase-controlled optical routing paths in a two-dimensional plane and thereby create photonic circuits at will, such as the examples shown in Figs. 1(b)–1(d). We anticipate this concept to be the starting point of transferring the inestimable enabling power of electrical FPGAs to photonic integrated circuits.

To give an experimental demonstration of this concept, we present here for the first time, to the best of our knowledge, such a programmable photonic chip. For a proof of principle, the layout comprises a maximally simplified yet fully versatile 2×1 mesh network with two cells. We show that the simple dual-cell circuit with a free spectral range (FSR) of 14 GHz and full parameter programmability enables RF filters featuring continuous, over-two-octave frequency coverage, i.e., 1.6–6 GHz, and variable passband shaping ranging from a 55 dB extinction notch filter to a 1.6 GHz bandwidth flat-top filter. Aiming for a new technology enabler, the results presented here pave the way for the realization of powerful photonic signal-processing engines that will play key roles in future high-bandwidth RF communication systems and networks.

2. DEVICE PRINCIPLE

Figure 1(a) depicts a general waveguide mesh network comprising $M \times N$ square mesh cells, with the MZ couplers being the intercell pathways. Each MZ coupler has 2×2 connection ports, so it can be simultaneously connected to up to four other MZ couplers that constitute the mesh network. We implement the MZ couplers with a phase-tuning element ϕ_U on the upper arm and ϕ_L on the lower arm as shown in Fig. 1(a). The transfer matrix parameters $c_{ij} = \mathrm{Out}_i/\mathrm{In}_j$ for such a coupler are

$$c_{11} = -c_{22} = -\mathrm{j}\exp(\mathrm{j}\phi_A)\cdot\sin(\phi_D)\cdot\exp(\mathrm{j}2\pi f\Delta\tau) \quad \text{(bar port)}, \tag{1}$$

$$c_{12} = c_{21} = -\mathrm{j}\exp(\mathrm{j}\phi_A)\cdot\cos(\phi_D)\cdot\exp(\mathrm{j}2\pi f\Delta\tau) \quad \text{(cross port)}, \tag{2}$$

where $\phi_A = (\phi_U + \phi_L)/2$ and $\phi_D = (\phi_U - \phi_L)/2$, respectively, govern the phase and coupling coefficient of its output ports, and $\exp(\mathrm{j}2\pi f\Delta\tau)$ represents the frequency-dependent phase shift caused by the propagation delay $\Delta\tau$ of the coupler. By controlling ϕ_D, an MZ coupler is able to function as an arbitrary-ratio coupler [$0 < \sin(\phi_D), \cos(\phi_D) < 1$], or function simply as a length of two-port waveguide with the coupler either in bar status [$\sin(\phi_D) = 1$ and $\cos(\phi_D) = 0$] or cross status [$\sin(\phi_D) = 0$ and $\cos(\phi_D) = 1$] as illustrated in Fig. 1(a). In the latter function, the cross–bar status of the MZ couplers determines the routing direction of the light from one such waveguide to the next in the mesh network, and the total length of a routing path can be defined by allowing the light to travel through a corresponding number of such waveguides. Figure 1(b) illustrates the basic circuit building blocks and their implementations in such a mesh network by programming the MZ couplers accordingly, including a 2×2 coupler, a length of two-port waveguide, and a circular waveguide loop. Based on this programming mechanism, one can synthesize various circuit topologies in the mesh network. Figure 1(c) illustrates the implementations of the two general types of waveguide filters that are commonly used to perform signal processing, namely, finite-impulse response filters based on tapped delay lines and infinite-impulse response filters based on ring resonators [32]. As far as the mesh network dimension allows, one can reach circuit topologies with arbitrarily extendable functionality, an example of which is depicted in Fig. 1(d). It is important to mention that next to the freedom in circuit topologies, ϕ_D in the couplers and ϕ_A in the constituent waveguides provide the defined circuits with full control capabilities of the amplitude and phase of the light, which facilitates the complete function programmability of the device.

Figure 2(a) presents a first-demonstrator chip with two mesh cells, fabricated in a commercial Si_3N_4 waveguide technology (TriPleX [33]; see Supplement 1). To simplify the fabrication, we use dedicated phase shifters and MZ couplers with a single phase-tuning element to perform, respectively, the effect of ϕ_A and ϕ_D of MZ couplers with two phase-tuning elements. The phase-tuning elements are implemented using resistor-based heaters, which cause a waveguide refractive index change by locally varying the waveguide temperature [10]. On this chip, the phase shifters are found with a full tuning range of 0–2π; the power coupling coefficient of the MZ couplers can be tuned very close to the ideal case, i.e., tunable between 0 and 0.99. By programming the values of the phase-tuning elements, we demonstrate four distinctively different circuit configurations, including a single-ring notch filter [34], a single-ring Hilbert transformer [35], a dual-ring bandpass filter [36], and a dual-ring delay line [37]. The corresponding settings of the chip and the measurements of the frequency response shapes that verify the circuit functionalities are depicted in Fig. 2(b).

3. RF FILTER IMPLEMENTATION

Using the demonstrator chip as a programmable photonic signal processor, we implement a new microwave photonic approach of generating RF filters. A schematic of the system and an illustration of the working principle are presented in Fig. 3. Here, an electro-optic modulator is used to create a double-sideband modulation

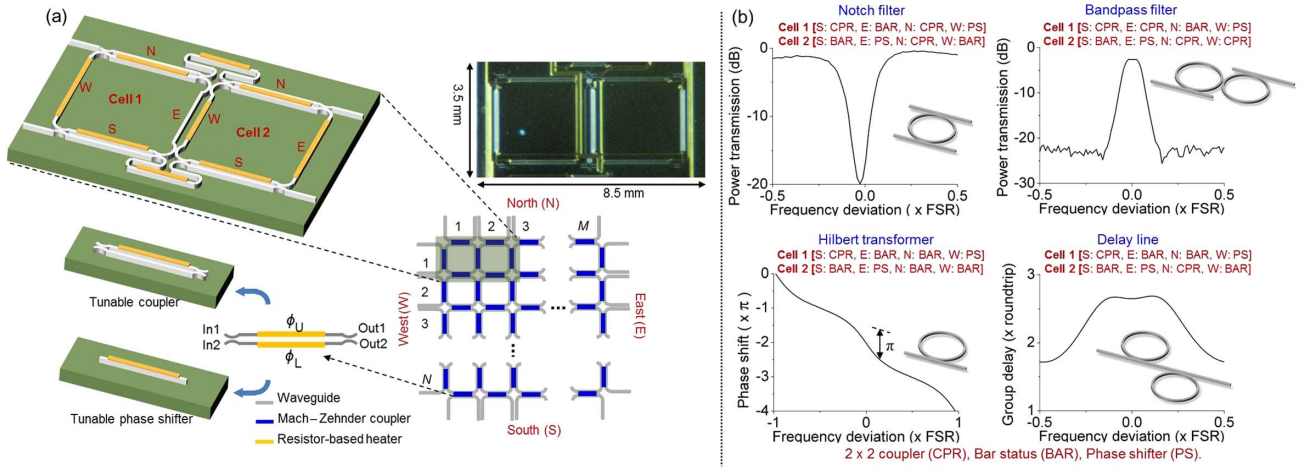

Fig. 2. (a) Schematic and a photo of the demonstrator chip fabricated using a commercial Si_3N_4 waveguide technology (TriPleX). (b) Four different circuit configurations created by programming the phase-tuning elements in the chip and the measurements of their corresponding frequency response shapes.

spectrum from an input RF signal under a small signal condition [38,39]. The chip is programmed into a circuit comprising a cascade of two ring resonators [as the delay line in Fig. 2(b)], whose resonance frequency and resonance strength are controllable via phase shifters ϕ_n and couplers κ_n, respectively, [32]. We program the two ring resonators such that Ring 1 and Ring 2 have their resonance frequencies in the upper and lower modulation sidebands, respectively, and both feature a sharp phase transition and a significant amplitude notch around the resonance frequency and nearly flat phases and amplitudes outside (for simplicity, we consider here only the resonance effect for normal dispersions [32]). The equivalent RF responses of the two sidebands after direct detection are depicted alongside, assuming a high-speed photodetector providing sufficient RF bandwidth. The highlighted area exhibits a frequency region where the two RF responses have nearly equal amplitudes and a phase difference of π, in contrast to the equal-phase areas on its two sides.

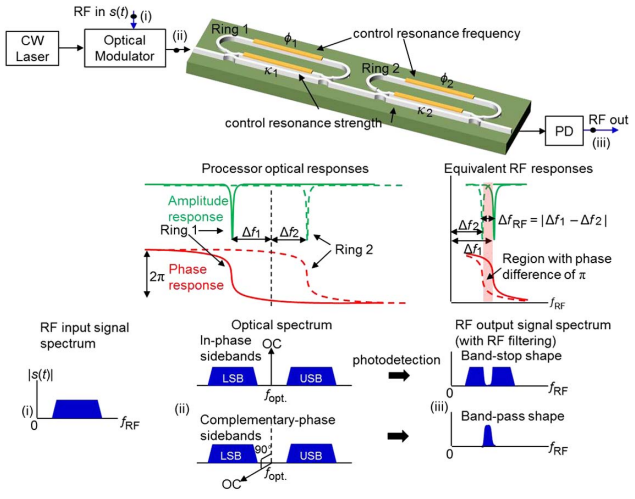

Fig. 3. Schematic of the microwave photonic system and an illustration of the working principle to implement an RF filter (CW, continuous wave; LSB/USB, lower/upper sideband; OC, optical carrier; PD, photodetection).

Eventually, these two RF responses add up vectorially at the photodetector output, resulting in an RF filter as illustrated in Fig. 3: a band-stop filter or a bandpass filter, depending on the phase relation between the optical carrier and the sidebands at the modulator output. In practice, a dual-parallel MZ modulator can be used to provide the desired optical spectrum with either in-phase or complementary-phase sidebands (Fig. 3) by controlling the modulator biases [40,41]. Moreover, the programmability of the chip also allows us to implement an RF filter using a conventional microwave photonic approach based on single-sideband modulation [42], where the chip is programmed into an optical filter [e.g., a notch filter as in Fig. 2(b)]. Although also easy to implement, this conventional approach requires an additional processing step to remove one modulation sideband, which increases the system complexity and leads to an extra 3 dB loss in the system gain.

To verify the approach illustrated in Fig. 3, measurements of RF filter responses were performed for both the band-stop and bandpass cases (see Supplement 1). In Figs. 4(a) and 4(b), the measurements show clearly that a band-stop and a bandpass filter can be generated, both having passband–stopband extinctions >17 dB and passband dispersions <2 ps/MHz. The fitted curves show that the measured filter shapes are consistent with the theoretical filter transfer function (see Supplement 1). In Figs. 4(c) and 4(d), we demonstrate continuous tuning of the filter center frequency without changes in filter shape. This is performed by controlling the phase shifters (ϕ_1, ϕ_2) of the two ring resonators such that Δf_1 and Δf_2 (as referred to in Fig. 3) are shifted simultaneously with a constant $\Delta f_{RF} = |\Delta f_1 - \Delta f_2|$. Subject to the frequency periodicity of ring resonators, the maximum frequency coverage of the RF filter equals half of the ring resonator FSR, that is, 14 GHz in this case. Here, we demonstrate frequency tuning from 1.6 to 6 GHz (31% of the ring resonator FSR), showing a frequency coverage greater than two octaves. It is worth mentioning that a two-octave frequency coverage in combination with continuous frequency tuning is difficult to achieve with electronic RF filters [43–46]. Besides, our RF filter employs only two tuning elements (ϕ_1, ϕ_2) to perform frequency tuning, implying easy control.

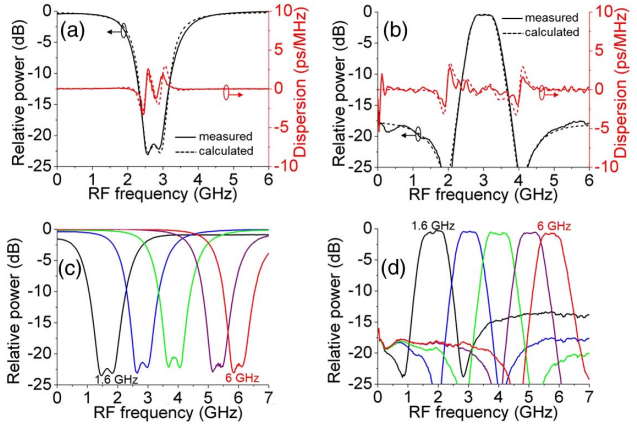

Fig. 4. (a, b) Measured band-stop and bandpass filter responses and fitted curves of the theoretical filter transfer function. (c, d) Demonstration of the continuous tuning of the filter center frequency.

Next to the continuous frequency tuning, the full control capabilities of the phase shifters (ϕ_1, ϕ_2) and couplers (κ_1, κ_2) of the two ring resonators also allow variable passband shaping. Figure 5 presents the measurements of many different filter responses ranging from a 55 dB extinction notch filter to a 1.6 GHz bandwidth flat-top filter. In Figs. 5(a) and 5(b), we demonstrate variable passband shaping by controlling the phase shifters (ϕ_1, ϕ_2). Unlike the operation for the filter center frequency tuning, Δf_1 and Δf_2 (as referred to in Fig. 3) are shifted independently in this case and the frequency difference of $\Delta f_{RF} = |\Delta f_1 - \Delta f_2|$ between them determines the width and ripple of the filter shape. This effect applies to both band-stop and bandpass type of filters. From a practical perspective, however, such as in flat-top filters, it is undesirable to increase the passband ripple when increasing the filter bandwidth. This issue can be addressed by an appropriate setting of the couplers (κ_1, κ_2), which is shown in the measurements in Fig. 5(c). We have achieved wideband flat-top filters with 1 dB bandwidth of up to 1.6 GHz (11% of the ring resonator FSR or, equally, 36% of the filter frequency coverage). In addition, when the two couplers (κ_1, κ_2) are set with identical coupling coefficients, a passband–stopband extinction of 25 dB can be reached, a measurement of which is shown in Fig. 5(d). Such RF filters with frequency agility and adjustable bandwidths have great application potential for high-spectrum-efficiency RF technologies such as cognitive radios [47].

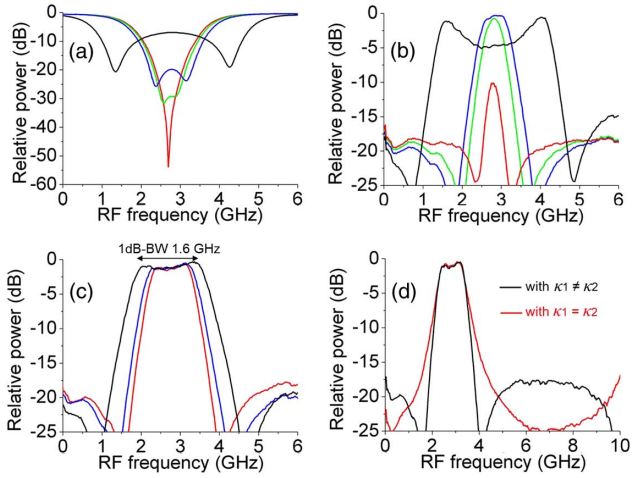

Fig. 5. (a), (b) RF filters with different widths and ripples by controlling only ϕ_1 and ϕ_2. (c) Flat-top filters with different bandwidths by controlling ϕ_1, ϕ_2, κ_1, and κ_2. (d) A flat-top filter with a passband–stopband extinction of 25 dB by setting $\kappa_1 = \kappa_2$.

4. DISCUSSION

The proper operation of such function-programmable photonic chips as described above relies on the tunability of the MZ couplers, which translates to stringent design requirements for the coupler phase and coupling coefficient tuning range. Our demonstrator chip features good tunability ($\phi = [0, 2\pi]$, $\kappa = [0, 0.99]$), but the complexity of the programmable circuit topologies (functions) are limited by the small dimension of the mesh network (two mesh cells). However, by scaling up the network dimension, a myriad of functions that are based on more complex circuit topologies are expected to be implementable, such as tapped-delay-line filters, multichannel (de)multiplexers and cross-connects, high-order coupled resonators, and various combinations of such circuits [32]. With sufficient space on the chip, it is also possible to implement multiple independent functionalities simultaneously, enabling a "multitask photonic processor."

In view of such significant promise, it is required as well to discuss what challenges would be raised in fabrication and operation when increasing the network dimensions. For one thing, increasing the network dimension means enlarging the chip area. In our case, where Si_3N_4 waveguides are employed for realizing a demonstrator, the chip carries MZ couplers with a length of 3450 μm at a group index of 1.71 (including a heater section with a length of 2100 μm and two 3 dB directional couplers, each having a length of 675 μm). This means area of about 0.35 cm × 0.35 cm for one mesh cell, which will, for instance, scale up by 100 times when aiming for a 10 × 10 mesh network. This bears higher risks of waveguide nonuniformity across the chip due to fabrication tolerance and may cause some degradation in device performance, such as via a limited tuning range of part of the couplers [32–36]. Regarding losses, the total device insertion loss includes the losses in the optical paths and coupling losses, in our case about 9 dB in total, dominated by two times the fiber-chip coupling loss of about 4 dB per facet (which is expected to decrease effectively when particular waveguide designs or interposers are used to minimize the mode–profile mismatch at the coupling). However, a large network dimension may incur increased losses due to the longer optical paths that are provided and due to possible power leakage at each coupler therein. Therefore, a low-loss waveguide technology is of great importance for system performance, particularly for RF applications where some processing schemes have the system loss in a quadratic relation with the optical loss [38]. Moreover, large network dimensions also mean a large number of tuning elements, the calibration and control of which require a considerable engineering effort due to possible initial offsets and interelement crosstalk. For device characterization and proper operation, dedicated power-monitoring ports can be implemented as part of a circuit topology alongside the targeted functions. In this work, a commercial 12-bit control subsystem (SATRAX B.V.) is used, which is sufficient to implement designed algorithms for circuit parameter configuration and

crosstalk compensation (yielding the results in Figs. 4 and 5). Further, when using thermo-optical tuning as is done here, a powerful chip temperature control setup may be required as the total heat dissipation of the chip scales with the number of tuning elements, causing a possible increase in the device size and weight. For the waveguide heaters in this work, an average power consumption of 0.25 W per heater is measured during operation, which is expected to be reduced by a factor of 5 when using optimized designs of the waveguide and heaters [24,33]. Many orders in power reduction might become available when implementing piezo tuning [48], or, using other platforms, implementing electro-optic tuning [11,19,23]. From a broad perspective, a general solution to address the above concerns is a low-loss waveguide technology that enables further device miniaturization through higher index contrast and provides index tuning with high power efficiency and on shorter length scales. In this regard, the silicon-on-insulator waveguide technology has shown interesting results [15,16,25,34–37], enabling tunable MZ couplers with lengths of tens of micrometers. This offers investigating the realization of the proposed waveguide mesh networks with more than an order-of-magnitude decrease in size (two orders in area). In addition, further device miniaturization also means that the FSRs of the circuits can be enlarged [32]. Our demonstrator chip is able to synthesize circuits with FSRs of the order of tens of GHz. Such FSRs are suitable for RF applications. A transition toward larger FSRs will considerably expand the application potential of such photonic signal processor chips, e.g., via tapped-delay-line equalizers, wavelength-division (de)multiplexing, and reconfigurable add–drop multiplexers, for optical communications [49].

Regarding RF filter implementation, we showed RF filter passbands with frequency resolution of the order of GHz. This can be further scaled down by means of an according increase of the FSR of the processor chip. However, in the case of a sharper frequency resolution, for instance of the order of tens of megahertz as required by mobile communication channels and satellite transponders [1,2], the quality of the CW laser is critical to the filter performance as the filter frequency stability relies largely on the laser linewidth and frequency jitter, which may be significant compared with the filter bandwidth. Promisingly, kilohertz-linewidth lasers have been demonstrated on chip [50], which could be a low-cost solution to address this concern. Other drift-like fluctuations in the system control could be overcome by means of high-resolution tuning and adaptive control algorithms. The chip in this work employs thermo-optical tuning, so the programming speed is limited to the range of milliseconds. However, this could be improved significantly by the advancing of modulator technologies, where state-of-the-art devices have demonstrated modulation speeds of the order of hundreds of picoseconds [51]. Moreover, our RF filter implementation is subject to the principle of a microwave photonic link [38]. This means that the same challenges with respect to system gain, noise figure, and dynamic range also exist. The key to overcome these challenges resides to a large extent in the advancing of optoelectronic components for the conversion between electrical and optical signals. With regard to these properties, promising results have been achieved in the past decade: system gain values larger than 10 dB have been demonstrated, besides noise figure values below 6 dB at frequencies beyond 10 GHz, using special, highly sensitive (low V_π) modulators and with novel detectors that can handle high currents [52].

Funding. Agentschap NL (NL Agency) (IPD12009); Australian Research Council (ARC) (FL13010041).

See Supplement 1 for supporting content.

REFERENCES

1. K. L. Du and M. N. S. Swamy, *Wireless Communication Systems: from RF Subsystems to 4G Enabling Technologies* (Cambridge University, 2010).
2. M. Golio, ed., *RF and Microwave Applications and Systems* (CRC Press, 2008).
3. S. L. Dexheimer, ed., *Terahertz Spectroscopy: Principles and Applications* (CRC Press, 2008).
4. A. Seeds, "Microwave photonics," IEEE Trans. Microwave Theory Tech. **50**, 877–887 (2002).
5. J. Capmany and D. Novak, "Microwave photonics combines two worlds," Nat. Photonics **1**, 319–330 (2007).
6. S. Iezekiel, ed., *Microwave Photonics: Device and Applications* (Wiley, 2009).
7. D. A. I. Marpaung, C. G. H. Roeloffzen, R. G. Heideman, S. Sales, and J. Capmany, "Integrated microwave photonics," Laser Photon. Rev. **7**, 506–538 (2013).
8. S. M. Kuo, B. H. Lee, and W. Tian, *Real-Time Digital Signal Processing: Implementations and Applications* (Wiley, 2006).
9. B. B. Guan, S. S. Djordjevic, N. K. Fontaine, L. Zhou, S. Ibrahim, R. P. Scott, D. J. Geisler, Z. Ding, and S. J. B. Yoo, "CMOS compatible reconfigurable silicon photonic lattice filters using cascaded unit cells for RF-photonic processing," IEEE J. Sel. Top. Quantum Electron. **20**, 8202110 (2014).
10. H. W. Chen, A. W. Fang, J. D. Peters, Z. Wang, J. Bovington, D. Liang, and J. E. Bowers, "Integrated microwave photonic filter on a hybrid silicon platform," IEEE Trans. Microwave Theory Tech. **58**, 3213–3219 (2010).
11. E. J. Norberg, R. S. Guzzon, J. S. Parker, L. A. Johansson, and L. A. Coldren, "Programmable photonic microwave filters monolithically integrated in InP–InGaAsP," J. Lightwave Technol. **29**, 1611–1619 (2011).
12. J. Lloret, G. Morthier, F. Ramos, S. Sales, D. Van Thourhout, T. Spuesens, N. Olivier, J.-M. Fédéli, and J. Capmany, "Broadband microwave photonic fully tunable filter using a single heterogeneously integrated III–V/SOI-microdisk-based phase shifter using high-*Q* silicon microdisk resonators," Opt. Express **20**, 10796–10806 (2012).
13. M. Ferrera, Y. Park, L. Razzari, B. E. Little, S. T. Chu, R. Morandotti, D. J. Moss, and J. Azaña, "On-chip CMOS-compatible all-optical integrator," Nat. Commun. **1**, 1–5 (2010).
14. F. Liu, T. Wang, L. Qiang, T. Ye, Z. Zhang, M. Qiu, and Y. Su, "Compact optical temporal differentiator based on silicon microring resonator," Opt. Express **16**, 15880–15886 (2008).
15. J. Wang, H. Shen, L. Fan, R. Wu, B. Niu, L. T. Varghese, Y. Xuan, D. E. Leaird, X. Wang, F. Gan, A. M. Weiner, and M. Qi, "Reconfigurable radio-frequency arbitrary waveforms synthesized in a silicon chip," Nat. Commun. **6**, 5957 (2015).
16. M. H. Khan, H. Shen, Y. Xuan, L. Zhao, S. Xiao, D. E. Leaird, A. M. Weinerm, and M. Qi, "Ultrabroad-bandwidth arbitrary radiofrequency waveform generation with a silicon photonic chip-based spectral shaper," Nat. Photonics **4**, 117–122 (2010).
17. J. S. Fandiño, J. D. Doménech, P. Muñoz, and J. Capmany, "Integrated InP frequency discriminator for phase-modulated microwave photonic links," Opt. Express **21**, 3726–3736 (2013).
18. D. A. I. Marpaung, C. G. H. Roeloffzen, A. Leinse, and M. Hoekman, "A photonic chip based frequency discriminator for a high performance microwave photonic link," Opt. Express **18**, 27359–27370 (2010).
19. J. Sancho, J. Bourderionnet, J. Lloret, S. Combrié, I. Gasulla, S. Xavier, S. Sales, P. Colman, G. Lehoucq, D. Dolfi, J. Campany, and A. De Rossi, "Integrable microwave filter based on a photonic crystal delay line," Nat. Commun. **3**, 1075 (2012).
20. L. Zhuang, M. Hoekman, W. P. Beeker, A. Leinse, R. G. Heideman, P. W. L. Van Dijk, and C. G. H. Roeloffzen, "Novel low-loss waveguide delay lines using Vernier ring resonators for on-chip multi-λ microwave photonic signal processors," Laser Photon. Rev. **7**, 994–1002 (2013).

21. A. Meijerink, C. G. H. Roeloffzen, R. Meijerink, L. Zhuang, D. A. I. Marpaung, M. J. Bentum, M. Burla, J. Verpoorte, P. Jorna, A. Hulzinga, and W. C. Van Etten, "Novel ring resonator-based integrated photonic beamformer for broadband phased-array antennas—Part I: design and performance analysis," J. Lightwave Technol. **28**, 3–18 (2010).
22. L. Zhuang, C. G. H. Roeloffzen, A. Meijerink, M. Burla, D. A. I. Marpaung, A. Leinse, M. Hoekman, H. G. Heideman, and W. C. Van Etten, "Novel ring resonator-based integrated photonic beamformer for broadband phased-array antennas—Part II: experimental prototype," J. Lightwave Technol. **28**, 19–31 (2010).
23. M. Smit, J. Van der Tol, and M. Hill, "Moore's law in photonics,"Laser Photon. Rev. **6**, 1–13 (2012).
24. C. G. H. Roeloffzen, L. Zhuang, C. Taddei, A. Leinse, R. G. Heideman, P. W. L. Van Dijk, M. Oldenbeuving, D. A. I. Marpaung, M. Burla, and K.-J. Boller, "Silicon nitride microwave photonic circuits," Opt. Express **21**, 22937–22961 (2013).
25. R. Soref, "The past, present and future of silicon photonics," IEEE J. Sel. Top. Quantum Electron. **12**, 1678–1687 (2006).
26. M. R. Heck, J. F. Bauters, M. L. Davenport, J. K. Doylend, S. Jain, G. Kurczveil, S. Srinivasan, Y. Tang, and J. E. Bowers, "Hybrid silicon photonic integrated circuit technology," IEEE J. Sel. Top. Quantum Electron. **19**, 6100117 (2013).
27. M. Burla, M. Li, L. R. Cortés, X. Wang, M. R. Fernández-Ruiz, L. Chrostowski, and J. Azaña, "Terahertz-bandwidth photonic fractional Hilbert transformer based on a phase-shifted waveguide Bragg grating on silicon," Opt. Lett. **39**, 6241–6244 (2014).
28. J. Capmany, D. Domenéch, and P. Muñoz, "Graphene integrated microwave photonics," J. Lightwave Technol. **32**, 3785–3796 (2014).
29. D. A. I. Marpaung, B. Morrison, M. Pagani, R. Pant, D. Y. Choi, B. Luther-Davies, S. J. Madden, and B. J. Eggleton, "Low-power, chip-based stimulated Brillouin scattering microwave photonic filter with ultrahigh selectivity," Optica **2**, 76–83 (2015).
30. S. Trimberger, *Field-Programmable Gate Array Technology* (Springer, 1994).
31. D. Pérez, I. Gasulla, and J. Capmany, "Software-defined reconfigurable microwave photonics processor," Opt. Express **23**, 14640–14654 (2015).
32. C. K. Madsen and J. H. Zhao, *Optical Filter Design and Analysis: a Signal Processing Approach* (Wiley, 1999).
33. K. Wörhoff, R. G. Heideman, A. Leinse, and M. Hoekman, "TriPleX: a versatile dielectric photonic platform," Adv. Opt. Technol. **4**, 189–207 (2015).
34. W. Bogaerts, P. De Heyn, T. Van Vaerenbergh, K. De Vos, S. Kumar Selvaraja, T. Claes, P. Dumon, P. Bienstman, D. Van Thourhout, and R. Baets, "Silicon microring resonator," Laser Photon. Rev. **6**, 47–73 (2012).
35. H. Shahoei, P. Dumais, and J. P. Yao, "Continuously tunable photonic fractional Hilbert transformer using a high-contrast germanium-doped silica-on-silicon microring resonator," Opt. Lett. **39**, 2778–2781 (2014).
36. F. Morichetti, C. Ferrari, A. Canciamilla, and A. Melloni, "The first decade of coupled resonator optical waveguide: bringing slow light to applications," Laser Photon. Rev. **6**, 74–96 (2012).
37. J. Cardenas, M. A. Foster, N. Sherwood-Droz, C. B. Poitras, L. Hugo, R. Lira, B. Zhang, A. L. Gaeta, J. B. Khurgin, P. Morton, and M. Lipson, "Wide-bandwidth continuously tunable optical delay line using silicon microring resonators," Opt. Express **18**, 26525–26534 (2010).
38. C. H. Cox III, *Analog Optical Links* (Cambridge University, 2004).
39. J. Capmany, B. Ortega, and D. Pastor, "A tutorial on microwave photonic filters," J. Lightwave Technol. **24**, 201–229 (2006).
40. W. Li, N. H. Zhu, L. X. Wang, J. S. Wang, J. G. Liu, Y. Liu, X. Q. Qi, L. Xie, W. Chen, X. Wang, and W. Han, "True-time delay line with separate carrier tuning using dual-parallel MZM and stimulated Brillouin scattering-induced slow light," Opt. Express **19**, 12312–12324 (2011).
41. L. Zhuang, C. Zhu, B. Corcoran, and A. J. Lowery, "Photonic high-bandwidth RF splitter with arbitrary amplitude and phase offset," Photon. Technol. Lett. **26**, 2122–2125 (2014).
42. A. Perentos, F. Cuesta-Soto, A. Canciamilla, B. Vidal, L. Pierno, N. S. Losilla, F. Lopez-Royo, A. Melloni, and S. Iezekiel, "Using Si_3N_4 ring resonator notch filter for optical carrier reduction and modulation depth enhancement in radio-over-fiber links," IEEE Photon. J. **5**, 5500110 (2013).
43. J. Long, C. Li, W. Cui, J. Huangfu, and L. Ran, "A tunable microstrip band-pass filter with two independently adjustable transmission zeros," IEEE Microwave Wireless Compon. Lett. **21**, 74–76 (2011).
44. A. Velez, F. Aznar, M. Durán-Sindreu, J. Bonache, and F. Martin, "Tunable coplanar waveguide band-stop and band-pass filters based on open split ring resonators and open complementary split ring resonators," IEEE Microwaves Antennas Propag. **5**, 277–281 (2011).
45. V. Sekar, M. Armendariz, and K. Entesari, "A 1.2–1.6-GHz substrate-integrated-waveguide RF MEMS tunable filter," IEEE Trans. Microwave Theory Tech. **59**, 866–876 (2011).
46. M. R. Rafique, T. Ohki, B. Banik, H. Engseth, P. Linner, and A. Herr, "Miniaturized superconducting microwave filters," Supercond. Sci. Technol. **21**, 075004 (2008).
47. B. A. Fette, ed., *Cognitive Radio Technology* (Elsevier, 2009).
48. N. Hosseini, R. Dekker, M. Hoekman, M. Dekkers, J. Bos, A. Leinse, and R. Heideman, "Stress-optic modulator in TriPleX platform using a piezoelectric lead zirconate titanate (PZT) thin film," Opt. Express **23**, 14018–14026 (2015).
49. A. Willner, S. Khaleghi, M. R. Chitgarha, and O. F. Yilmaz, "All-optical signal processing," J. Lightwave Technol. **32**, 660–680 (2014).
50. R. M. Oldenbeuving, E. J. Klein, H. L. Offerhaus, C. J. Lee, H. Song, and K.-J. Boller, "25 kHz narrow spectral bandwidth of a wavelength tunable diode laser with a short waveguide-based external cavity," Laser Phys. Lett. **10**, 015804 (2013).
51. Q. Xu, B. Schmidt, S. Pradhan, and M. Lipson, "Micrometre-scale silicon electro-optic modulator," Nature **435**, 325–327 (2005).
52. E. I. Ackerman, G. Betts, W. K. Burns, J. C. Campbell, C. H. Cox III, N. Duan, J. L. Prince, M. D. Regan, and H. V. Roussell, "Signal-to-noise performance of two analog photonic links using different noise reduction techniques," in *IEEE/MTT-S International Microwave Symposium* (IEEE, 2007), pp. 51–54.